Hindawi
International Journal of Photoenergy
Volume 2020, Article ID 5039192, 8 pages
https://doi.org/10.1155/2020/5039192

Research Article

Laminating Fabrication of Bifacial Organic-Inorganic Perovskite Solar Cells

Yujing Yang, Yue Zhu, Xiaoxiao Wang, Qi Song, Chao Ji, Huimin Zhang, Zhiqun He, and Chunjun Liang

Key Laboratory of Luminescence and Optical Information, Ministry of Education, School of Science Beijing Jiaotong University, Beijing 100044, China

Correspondence should be addressed to Chunjun Liang; chjliang@bjtu.edu.cn

Received 4 September 2019; Revised 5 December 2019; Accepted 17 December 2019; Published 2 January 2020

Academic Editor: Věra Cimrová

Bifacial solar cells based on organic-inorganic perovskite are fabricated with a laminating process. The structure of the devices is ITO/SnO_2/$CH_3NH_3PbI_3$/NiO_x/ITO, in which both electrodes are the transparent ITO layer. Therefore, the device can receive light from both sides. By laminating the two half-devices, ITO/SnO_2/$CH_3NH_3PbI_3$ and $CH_3NH_3PbI_3$/NiO_x/ITO, at high temperature with pressure, the merging of the middle perovskite layers is enhanced. The optimized bifacial PSCs show a Voc of 0.85 V, FF of 0.58, Jsc of 17.53 mA/cm^2, and PCE of 8.47%. The photovoltaic performance varies when the light is illuminated from different sides of the bifacial PSCs. With illumination from the SnO_2 side, the Voc and Jsc of the PSCs are apparently higher than those from the NiO_x side, suggesting more severe electron-hole recombination at the NiO_x/perovskite interface than at the SnO_2/perovskite interface.

Organic-inorganic hybrid perovskite solar cells (PSCs) have received extensive attentions because of their prominent photoelectric properties, high carrier mobility, low exciton binding energies, and long diffusion length [1–3]. Device lifetime and power conversion efficiency (PCE) are the key factors determining the final cost of the electricity that solar cells generate. The certified PCE of perovskite solar cells (PSCs) has rapidly reached 23.7% over the past few years [4–7], which is comparable with that of silicon solar cells. However, the hybrid halides have poor tolerances under persistent attacks by moisture and heat, making improved device stability a challenging problem. The poor durability mainly arises from the ion-typed crystal structure and unstable consolidation of iodide ions [8], making hybrid halides destroyable by polar solvents, thermal attacks, and iodide diffusion [9]. Moreover, the high cost of state-of-the-art hole-transporting materials and gold electrodes has been an economical burden for their commercial applications [10].

Conventional PSCs usually consist of nontransparent electrodes. Therefore, the metal plating apparatus can only illuminate on the one side (Figure 1(a)). When a large number of single-sided solar panels are arranged neatly, some of the light incident on the front side of the panel is reflected to the back of the other panel, but these rays of sunlight cannot be reused. Therefore, these PSC panels can only collect solar energy from the side with transparent electrode, resulting in insufficient utilization of light.

We demonstrate here bifacial PSCs with ITO/SnO_2/$CH_3NH_3PbI_3$/NiO_x/ITO configuration, in which both electrodes are transparent. The front and rear transport layers share a single $CH_3NH_3PbI_3$ film. It is self-encapsulated with simple processes and materials, which overcame the difficulty in selecting proper and expensive electron and hole transport layers. It received illumination from both sides (Figure 1(b)).

Indium tin oxide- (ITO-) coated glass substrates were first cleaned with detergent, deionized water, and ethyl alcohol successively and then dried on a hot plate. The substrate was then treated with UV/ozone for 20 min for further cleaning. SnO_2 was dissolved in deionized water and stirred at room temperature for more than 12 h and then spin-coated at 3000 rpm/min for 40 s and annealed at 150°C for 10 min

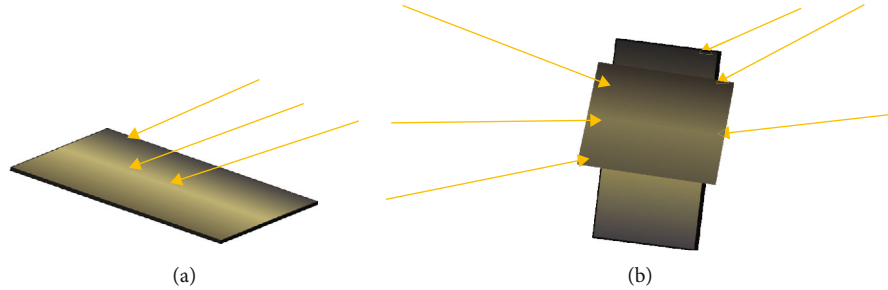

(a) (b)

Figure 1: Schematic diagram of PSCs under illumination: (a) conventional PSCs; (b) bifacial PSCs.

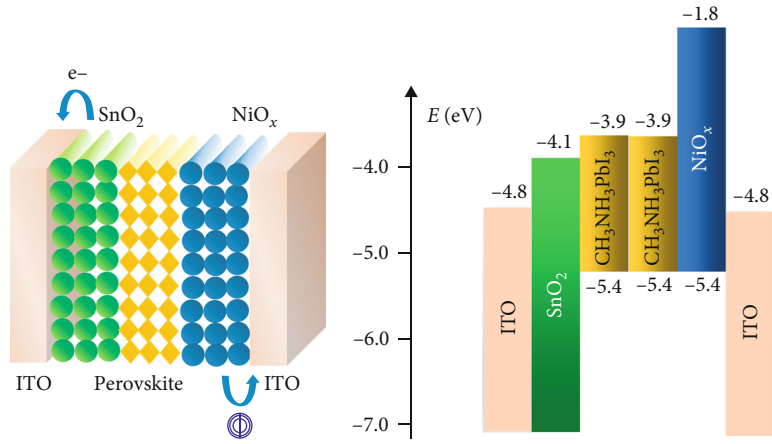

(a) (b)

Figure 2: Device structures: (a) schematic diagram of a bifacial PSC with ITO/SnO_2/$CH_3NH_3PbI_3$/NiO_x/ITO configuration; (b) energy band diagram of a bifacial PSC.

in air. NiO_x was dissolved in deionized water and stirred at 60°C for more than 12 h and then spin-coated at 3000 rpm/min for 40 s in air. Equal molar amounts of PbI_2 and MAI were mixed and dissolved in the solvent, which consisted of γ-butyrolactone (GBL) and dimethyl sulfoxide (DMSO) (8 : 2 *v*/*v*), and then stirred at 60°C over 12 h. The samples were moved into a vacuum chamber. The mixture solution was spin-coated separately onto SnO_2 and NiO_x substrates at 1000 rpm/min for 15 s and 3000 rpm/min for 35 s successively, followed by annealing on a hot plate at 100°C for 10 min in a nitrogen-filled glove box. The thickness of the perovskite film is about 200 nm. We applied pressure via a hand-operated vertical hydraulic jack. The assembly was put under a hotplate at 200°C. The pressure and temperature were held for 10 min and then unloaded. The perovskite film on the two glass substrates is tightly contacted and merged together. Both ends are clamped with a clamp. The cell area was 0.038 cm^2.

The device structure of the bifacial PSCs is shown in Figure 2(a). The structure of the devices is ITO/SnO_2/$CH_3NH_3PbI_3$/NiO_x/ITO, in which SnO_2 acts as an electron transport layer and NiO_x is the hole transport layer. The organic-inorganic perovskite $CH_3NH_3PbI_3$ is the light absorber. The energy band diagram of the bifacial PSCs is shown in Figure 2(b).

The LUMO level of SnO_2 matches that of the perovskite absorber, so that the photogenerated electrons in the perovskite can be efficiently collected and transported to the adjacent cathode. On the other hand, it has low HOMO level, which can effectively block holes from reaching the adjacent ITO electrode. Likewise, the HOMO level of NiO_x matches that of the perovskite absorber, so that the photogenerated holes in the perovskite can be efficiently collected and transported to the adjacent anode. Meanwhile, it has high LUMO level, which can effectively block electrons from reaching the anode. Therefore, the carrier selectivity of the charge transport layer determines the polarity of our bifacial PSCs in which both cathode and anode are a transparent ITO layer.

The fabrication process of the bifacial PSCs is shown in Figure 3. Firstly, we fabricate two half-devices as shown in Figure 3(a).

The electron (hole) transport layer SnO_2 (NiO_x) is spin-coated on the glass/ITO substrate, SnO_2 solution is made of high concentration of SnO_2 solution and deionized water, and the concentration is 200 mL/1 L, with stirring 12 hours at room temperature. NiO_x solution is made of NiO_x powder and deionized water, with concentration of 24 mg/1300 mL and stirring for 12 h at 60°C, and cleaned with an ultrasonic cleaner for 20 minutes before use. Both the SnO_2 and NiO_x solutions are rotated at 3000 r/min for 40 minutes;

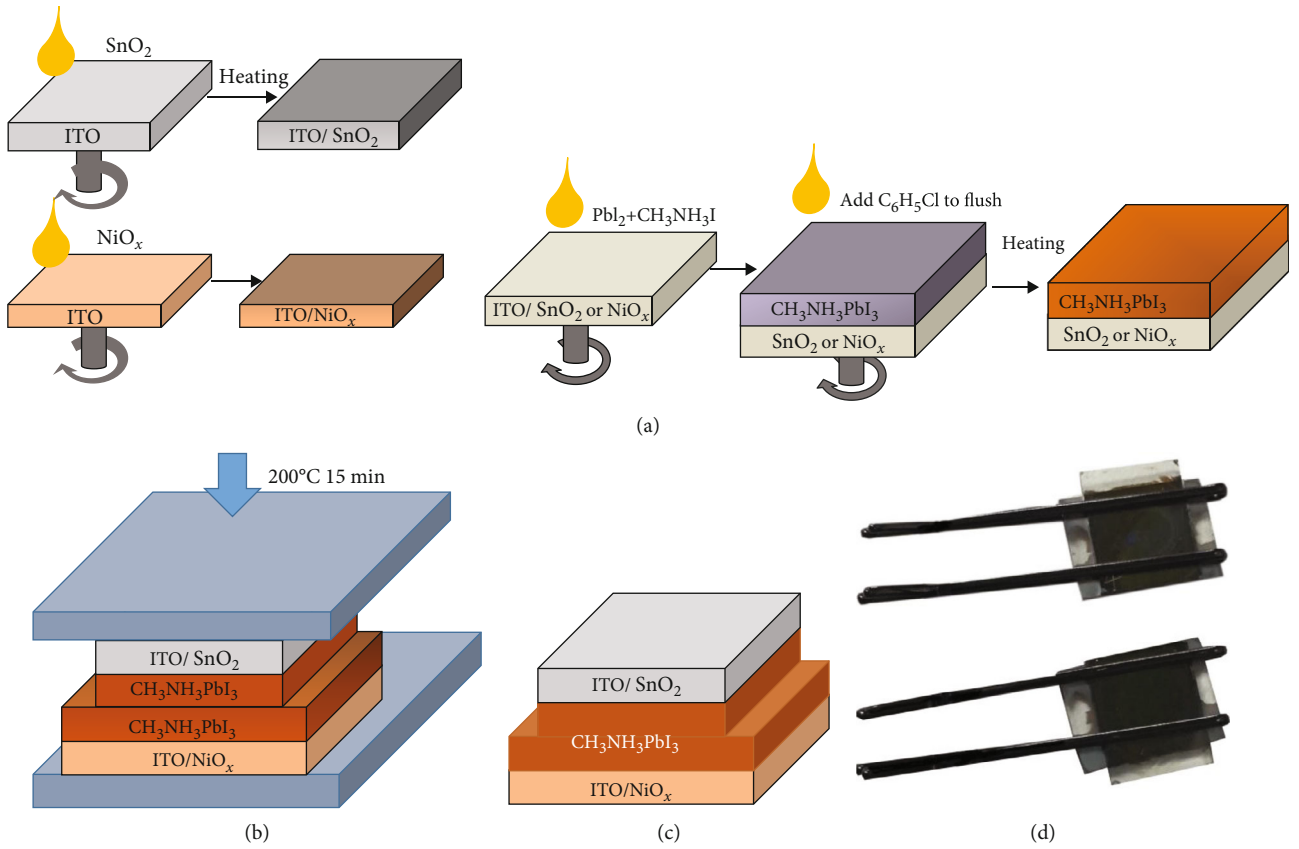

FIGURE 3: Flow chart of bifacial PSCs: (a) deposition perovskite film on the SnO_2 and NiO_x substrate, respectively; (b) lamination of the substrates together with pressure at 200°C for 15 min; (c) final device with perovskite films merging together; (d) photography of the devices.

furthermore, SnO_2 solutions need to be annealed for 10 min at 150°C after spinning. Then, the perovskite $CH_3NH_3PbI_3$ layer is deposited onto the electron (hole) transport layer with a one-step approach to finish the half-device, which is labeled as the ITO/SnO_2 (ITO/NiO_x) substrate. The perovskite solution is prepared by a one-step method, and the solute is PbI_2 and CH_3NH_3I. The solvents are 1 : 1 mixed with γ-butyrolactone and dimethyl sulfoxide, with stirring for 12 hours at 60°C and then filtering. Preheat at 60°C before use. We performed spin coating with the perovskite solution in two pieces of the ITO substrate in the nitrogen-filled glove box. The perovskite precursor was spin-coated on the substrate in a two-speed sequence: 1000 rpm for 15 s, followed by 3000 rpm for 35 s, and then an antisolvent chlorobenzene was poured onto the spinning substrate at moment of 25 s. Finally the substrate was annealed at 100°C for 10 min. Next, the ITO/SnO_2 and ITO/NiO_x substrates are laminated together to fabricate the bifacial PSCs with the application of pressure at elevated temperature (Figure 3(b)). After the lamination process, the separated perovskite layers at the middle part of the device are merged into one layer (Figure 3(c)). Figure 3(d) is the photographs of the final bifacial PSCs which are held with clips to prevent the unclasping of the device in the upcoming measurement.

The AFM images in Figures 4(a) and 4(b) show the morphology of the perovskite surface on the SnO_2/perovskite and NiO_x/perovskite substrate, respectively. The film surfaces are rough and uneven. When laminating the two half-devices together, the contact area between the middle perovskite layers may be very small due to the uneven surface of the perovskite layer on each substrate as illustrated in Figure 4(c).

The application of pressure and high temperature may change the contacting surfaces of the soft perovskite material and eventually merge the two perovskite layers into one layer (Figure 4(d)). Based on this conjecture, we investigated the effects of temperature and pressure on the performance of the bifacial PSCs.

At the constant pressure of 42 kPa, we explored the effect of temperature on the performance of the PSCs during the lamination process. As shown in Figure 5, when the temperature in the lamination process is changed from 160°C to 220°C, the Jsc, Voc, and fill factor all vary with the increasing temperature. In particular, the Jsc shows a clear sign of rising first and then decreasing, reaching a maximum at 200°C. As a result, the power conversion efficiency also displays a similar trend, reaching the highest value at 200°C. The results indicate that the merging of the perovskite layers is facilitated by the application of high temperature in the lamination process. If the temperature is low, the original perovskite layers cannot fully merge together, and there is still an unfused part that makes the two separate perovskite layers insufficiently contacted. In this case, the contact area in the perovskite interface is low, leading to low Jsc of the PSCs. At the

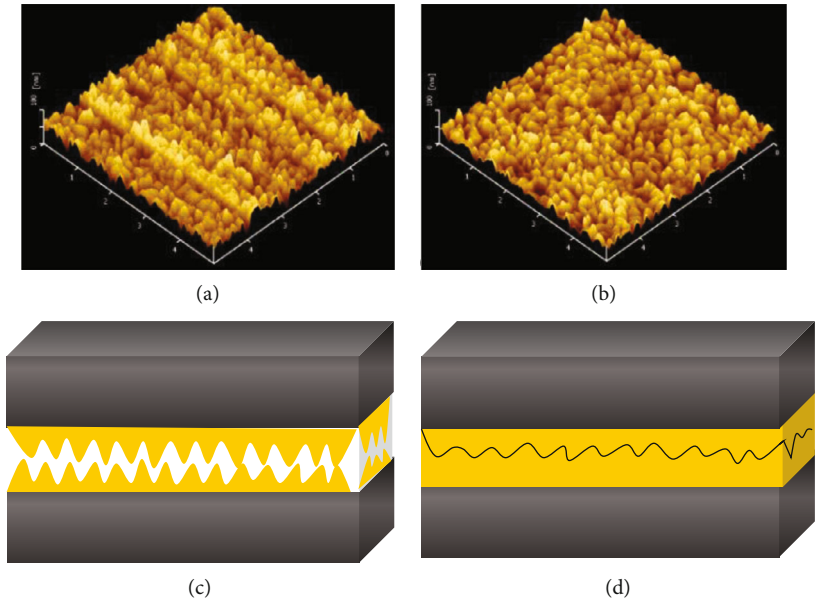

Figure 4: Surface topography of the perovskite layer and the merging of the intermediate perovskite layers during the lamination process: (a) AFM surface topography of the perovskite layer on the SnO_2 substrate; (b) AFM surface topography of the perovskite layer on the NiO_x substrate; (c) schematics showing the perovskite films before lamination with pressure and heating; (d) schematics showing the middle perovskite layers merging together after lamination.

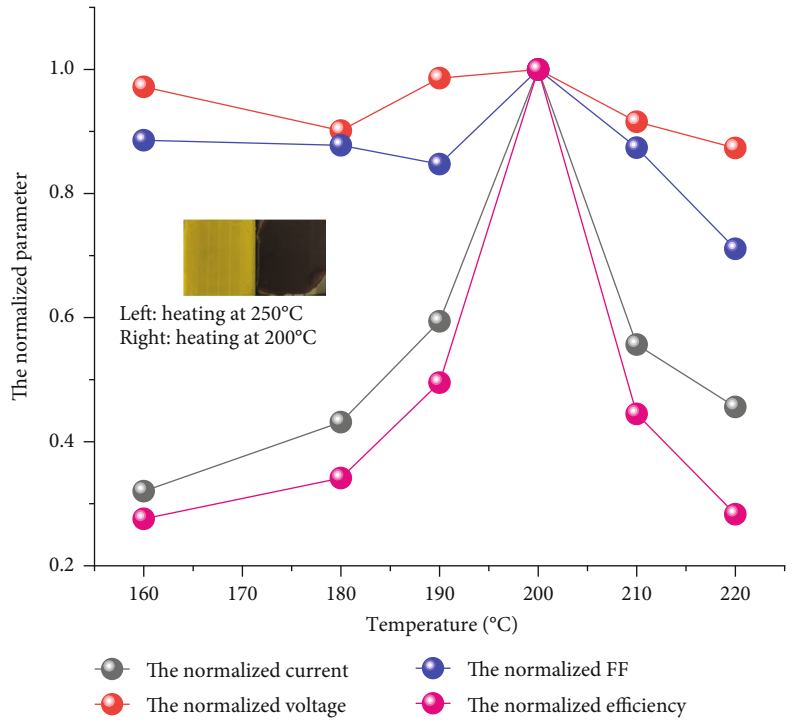

Figure 5: The dependence of the device performance on the applied temperature during the lamination.

elevated temperature, e.g., 200°C, the merging of the perovskite layers is enhanced, leading to an improved contact area and Jsc.

However, if the temperature is too high, the structure of the perovskite itself may become unstable because $CH_3NH_3^+$ has temperature-dependent high fluidity, which affects the irregular arrangement of $CH_3NH_3^+$ in the crystal structure. At high temperature, the binding stability of $CH_3NH_3^+$ decreases, and thus, a large number of $CH_3NH_3^+$ molecules undergo decomposition [11], resulting in deterioration of device performance. Figure 5 inset photos show that perovskite turns yellow quickly at high temperatures. This

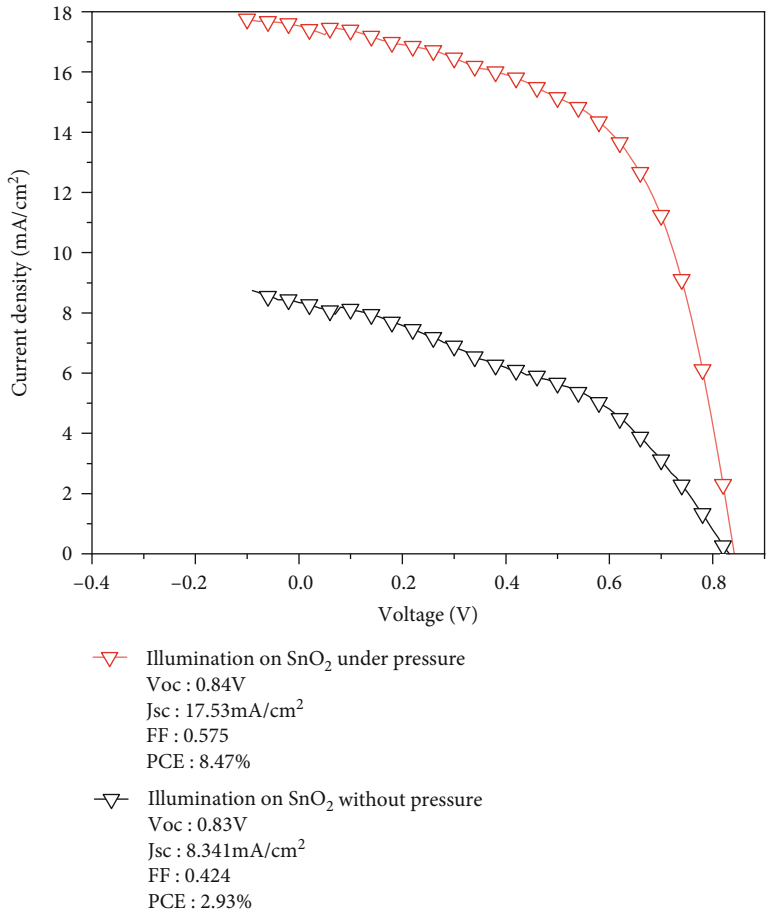

Figure 6: Effect of pressure on device performance.

indicates that high temperature does destroy the structure of perovskite and confirms our conjecture.

The pressure applied in the lamination process is found to be helpful for perovskite merging. A comparison of the device performance between the devices with and without pressure in the laminating process is shown in Figure 6. The laminated PSCs without pressing during fabrication show a Voc of 0.83 V, FF of 0.42, Jsc of 8.34 mA/cm^2, and PCE of 2.93%. The laminated PSCs with the pressure of 42 kPa show a Voc of 0.85 V, FF of 0.58, Jsc of 17.53 mA/cm^2, and PCE of 8.47%. The significantly increased Jsc and PCE in the latter device indicate the increased contact area and improved merging of the two-half devices with pressure.

It is found that the photovoltaic performance is different when the light is illuminated from different sides of the bifacial PSCs.

Figure 7(a) shows current-voltage characteristics when the PSCs are illuminated on the SnO_2 and NiO_x side, respectively. With illumination from the SnO_2 side, the Voc and Jsc of the PSCs are apparently larger than those from the NiO_x side. Therefore, the biface device shows higher PCE when it is illuminated from the SnO_2 side. This trend is verified in multiple devices. Figure 7(b) shows the statistics of the photovoltaic parameters, Voc, Jsc, FF, and PCE, in multiple devices. The result confirms that the bifacial PSCs demonstrate higher Voc, Jsc, and PCE when illuminated from the SnO_2 side other than the NiO_x side.

Figure 8(a) shows the absorption spectra of the bifacial PSCs illuminated from the SnO_2 and NiO_x side, respectively. The absorbance at the wavelength below the absorption edge (740 nm) is higher than unity. From the relation, Abs = − log (Transmittance) = − log (I_{out}/I_{in}), and the transmittance at the wavelength below 740 nm is less than 10%. The calculated profile of the intensity distribution with a transmittance of 10% is shown in Figure 8(b). When the incident light is on the SnO_2 side, the light intensity in the perovskite peaks at the SnO_2/perovskite interface and decreases quickly as the depth increases due to strong absorption of the perovskite film. Likewise, when the incident light is on the NiO_x side, the light intensity is strongest at the NiO_x/perovskite interface, and it becomes much weaker at the other side of the perovskite film. The light intensity profile also reflects the distribution of the photogenerated electron-hole pairs in the perovskite layer. Therefore, the different photovoltaic performances of the PSCs when illuminated from SnO_2 and from NiO_x sides suggest the different carrier dynamics at the two interfaces. The lower Voc and Jsc when illuminated on the NiO_x side compared with the SnO_2 side suggest more severe electron-hole recombination at the NiO_x/perovskite interface than at the SnO_2/perovskite

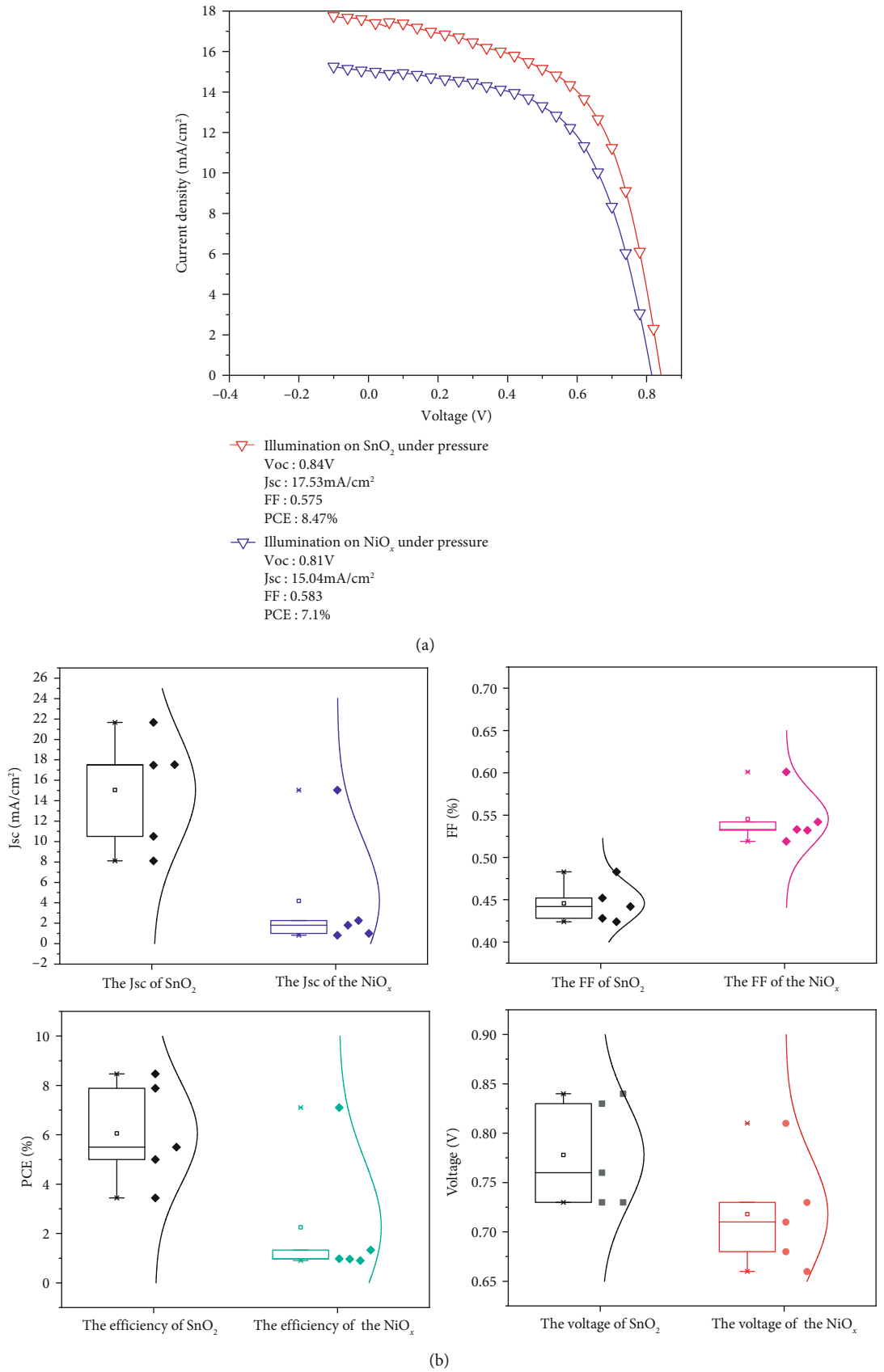

Figure 7: The different performances of the bifacial PSCs with illumination from different sides: (a) current-voltage characteristics of the PSCs; (b) statistics of the photovoltaic parameters in multiple devices.

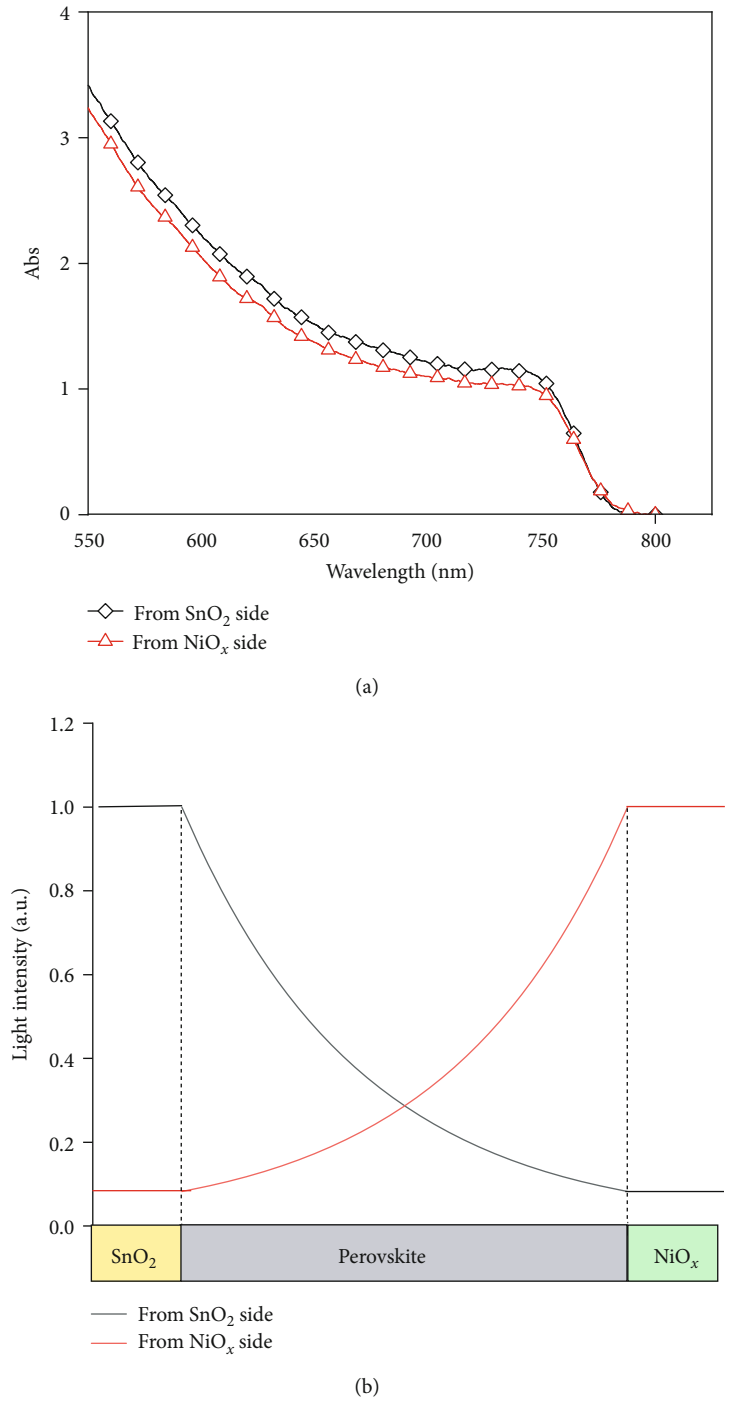

FIGURE 8: The absorption spectra and the light intensity distribution in the bifacial PSCs: (a) absorption spectra; (b) light intensity distribution with illumination from the SnO_2 and NiO_x sides, respectively. The light intensity profile in the perovskite also reflects the photogenerated carrier distribution.

interface. The reason is that the carrier collection and recombination are two competing processes in a photovoltaic device. A higher carrier recombination rate leads to lower collection efficiency of the PSCs, which directly result in lower Jsc. A higher recombination rate also results in a lower excessive carrier population in the perovskite layer, which leads to lower Voc.

1. Conclusion

In conclusion, the bifacial PSCs with the structure of ITO/SnO_2/$CH_3NH_3PbI_3$/NiO_x/ITO are fabricated. At the constant pressure of 42 kPa and at the elevated temperature of 200°C, the merging of the perovskite layers is enhanced, leading to an improved contact area and Jsc. The optimized

bifacial PSCs show a Voc of 0.85 V, FF of 0.58, Jsc of 17.53 mA/cm^2, and PCE of 8.47%. The photovoltaic performance is different when the light is illuminated from different sides of the bifacial PSCs. With illumination from the SnO_2 side, the Voc and Jsc of the PSCs are apparently larger than those from the NiO_x side. The result suggests more severe electron-hole recombination at the NiO_x/perovskite interface than at the SnO_2/perovskite interface.

Data Availability

The [DATA TYPE] data used to support the findings of this study are available from the corresponding author upon request.

Conflicts of Interest

The authors declare that they have no conflicts of interest.

Authors' Contributions

Yujing Yang, Yue Zhu, and Xiaoxiao Wang contribute equally to this work.

Acknowledgments

The authors acknowledge the financial support from the National Natural Science Foundation of China (Nos. 61874008, 61574014, and 11474017), Beijing Municipal Science and Technology Project (Z181100004718004), and Beijing Training Program of Innovation and Entrepreneurship for Undergraduates (Project 201910004168).

References

[1] S. D. Stranks, G. E. Eperon, G. Grancini et al., "Electron-Hole Diffusion Lengths Exceeding 1 Micrometer in an Organometal Trihalide Perovskite Absorber," *Science*, vol. 342, no. 6156, pp. 341–344, 2013.

[2] M. A. Green, A. Ho-Baillie, and H. J. Snaith, "The emergence of perovskite solar cells," *Nature Photonics*, vol. 8, no. 7, pp. 506–514, 2014.

[3] Q. Dong, Y. Fang, Y. Shao et al., "Electron-hole diffusion lengths > 175 μm in solution-grown $CH_3NH_3PbI_3$ single crystals," *Science*, vol. 347, no. 6225, pp. 967–970, 2015.

[4] A. Kojima, K. Teshima, Y. Shirai, and T. Miyasaka, "Organometal Halide Perovskites as Visible-Light Sensitizers for Photovoltaic Cells," *Journal of the American Chemical Society*, vol. 131, no. 17, pp. 6050-6051, 2009.

[5] M. M. Lee, J. Teuscher, T. Miyasaka, T. N. Murakami, and H. J. Snaith, "Efficient Hybrid Solar Cells Based on Meso-Superstructured Organometal Halide Perovskites," *Science*, vol. 338, no. 6107, pp. 643–647, 2012.

[6] H. Zhou, Q. Chen, G. Li et al., "Interface engineering of highly efficient perovskite solar cells," *Science*, vol. 345, no. 6196, pp. 542–546, 2014.

[7] J.-H. Im, I. H. Jang, N. Pellet, M. Grätzel, and N. G. Park, "Growth of $CH_3NH_3PbI_3$ cuboids with controlled size for high-efficiency perovskite solar cells," *Nature Nanotechnology*, vol. 9, no. 11, pp. 927–932, 2014.

[8] M. Yang, Y. Zhou, Y. Zeng, C. S. Jiang, N. P. Padture, and K. Zhu, "Square-Centimeter Solution-Processed Planar $CH_3NH_3PbI_3$ Perovskite Solar Cells with Efficiency Exceeding 15%," *Advanced Materials*, vol. 27, no. 41, pp. 6363–6370, 2015.

[9] O. Malinkiewicz, A. Yella, Y. H. Lee et al., "Perovskite solar cells employing organic charge-transport layers," *Nature Photonics*, vol. 8, no. 2, pp. 128–132, 2014.

[10] W. S. Yang, J. H. Noh, N. J. Jeon et al., "High-performance photovoltaic perovskite layers fabricated through intramolecular exchange," *Science*, vol. 348, no. 6240, pp. 1234–1237, 2015.

[11] W. S. Yang, B.-W. Park, E. H. Jung et al., "Iodide management in formamidinium-lead-halide–based perovskite layers for efficient solar cells," *Science*, vol. 356, no. 6345, pp. 1376–1379, 2017.